J Biol Inorg Chem (2011) 16:25–32
DOI 10.1007/s00775-010-0696-0

ORIGINAL PAPER

Phosphate ester cleavage promoted by a tetrameric iron(III) complex

Anob Kantacha · Rebecca Buchholz · Sarah J. Smith · Gerhard Schenk · Lawrence R. Gahan

Received: 17 May 2010 / Accepted: 12 August 2010 / Published online: 28 August 2010

Abstract The purple acid phosphatases (PAPs) are the only binuclear metallohydrolases where the necessity for a heterovalent active site [Fe(III)–M(II) (M is Fe, Zn or Mn)] for catalysis has been established. The paradigm for the construction of PAP biomimetics, both structural and functional, is that the ligands possess characteristics which mimic those of the donor sites of the metalloenzyme and permit discrimination between trivalent and divalent metal ions. The donor atom set of the ligand 2-((2-hydroxy-5-methyl-3-((pyridin-2-ylmethylamino)methyl)benzyl)(2-hydroxybenzyl)amino)acetic acid (H_3HPBA) mimics that of the active site of PAP although the iron(III) complex of this ligand has been characterized as the tetramer $[Fe_4(HPBA)_2(\mu\text{-}CH_3COO)_2(\mu\text{-}O)(\mu\text{-}OH)(OH_2)_2]ClO_4{\cdot}5H_2O$. The phosphoesterase-like activity of the complex in 1:1 acetonitrile/water has now been investigated using the substrate 2,4-bis(dinitrophenyl)phosphate. The pH dependence of the catalytic rate revealed a non-symmetric bell-shaped profile, with a finite but non-zero rate at high pH. Unlike the traditional approach usually employed to analyse these bell-shaped profiles, the approach used here involved incorporating additional species which contribute to the overall activity. Employing this approach, we show that the complex has a k_{cat} of 1.6 (±0.2) × 10^{-3} s^{-1}, three kinetically relevant pK_a values of 5.3, 6.2 and 8.4, with K_M of 7.4 ± 0.6 mM. The kinetic parameters are similar to those reported for heterovalent PAP biomimetics. Additionally, it is observed that, unlike the enzyme, the oxidation state is not the determining factor for catalytic activity.

Keywords Purple acid phosphatase · Phosphodiester-degrading enzyme · Binuclear metallohydrolases · Iron complexes · Biomimetics

A. Kantacha
Department of Chemistry,
Faculty of Science,
Thaksin University,
140 Tambon Koaroobchang,
Muang, Songkhla 90000, Thailand

R. Buchholz · S. J. Smith · G. Schenk · L. R. Gahan (✉)
School of Chemistry and Molecular Biosciences,
The University of Queensland,
St. Lucia, QLD 4072, Australia
e-mail: gahan@uq.edu.au

Introduction

Purple acid phosphatases (PAPs) are the only binuclear metallohydrolases where the necessity for a heterovalent active site [Fe(III)–M(II) (M is Fe, Zn or Mn)] for catalysis has been established [1, 2]. The enzyme isolated from mammals (pig, bovine, mouse, rat and human) is an approximately 35 kDa monomeric protein with an Fe(III)–Fe(II) centre, and a characteristic purple colour due to a charge-transfer transition (λ_{max} = 510–560 nm; ε = ~3,000–4,000 M^{-1} cm^{-1}) from a conserved tyrosine ligand to the ferric ion (Fig. 1) [3–5]. Mammalian PAPs are easily and reversibly oxidized to the inactive diferric form owing to the low redox potential (approximately 340 mV) of the divalent iron [6, 7], suggesting that the PAP activity may be regulated in vivo by reversible oxidation/reduction of the active site.

The paradigm for the construction of PAP biomimetics is that the ligands possess characteristics such that hard and soft coordination sites permit discrimination between the trivalent and divalent metal ions. The ligand 2-bis[((2-pyridylmethyl)aminomethyl)-6-((2-hydroxybenzyl)-(2-pyridylmethyl))-aminomethyl]-4-methylphenol (H_2BPBPMP;

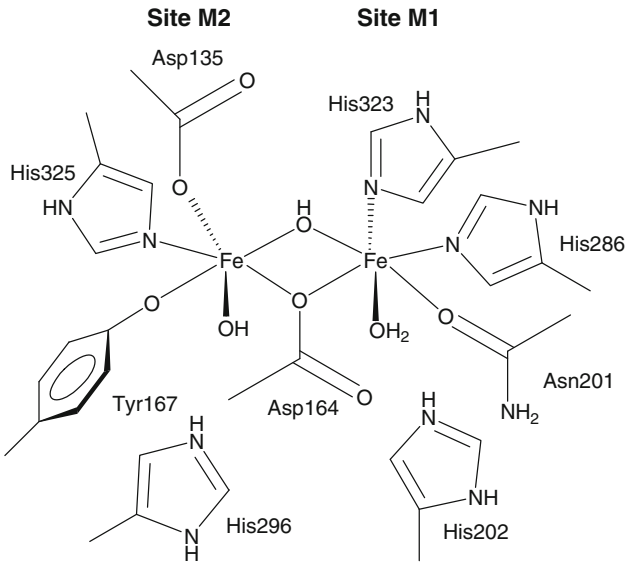

Fig. 1 Active site of mammalian purple acid phosphatase (PAP). Fe(III) binds to the high-affinity metal site M2 and Fe(II) is bound to the low-affinity site M1. The seven metal-ion-coordinating residues and the two histidines (His202 and His296) are highly conserved among PAPs from different sources. Tyr167 forms a charge-transfer complex with Fe(III) [1]

Fig. 2) is able to selectively generate heterobinuclear $[Fe(III)(\mu\text{-}CH_3COO)_2(\mu\text{-phenoxide})M(II)]^+$ complexes, effectively structurally mimicking the PAP active site [8]. Phosphatase activities of the Fe(III)–M(II) (M is Mn, Co, Ni, Cu or Zn) complexes of $BPBPMP^{2-}$ have been measured with the activated substrate 2,4-bis(dinitrophenyl) phosphate (BDNPP) [9–11]. These reactions are strongly dependent on pH, giving rise to bell-shaped pH versus rate profiles and pH optima in the range 6.0–7.0 [10–14]. In each case the catalytically active species is proposed to be of the type $[(OH)Fe(III)(\mu\text{-}OH)M(II)(OH_2)]$ [1].

We previously reported the characterization of a tetrameric Fe(III) complex of the ligand 2-((2-hydroxy-5-methyl-3-((pyridin-2-ylmethylamino)methyl)benzyl)(2-hydroxybenzyl)amino)acetic acid (H_3HPBA; Fig. 2), $[Fe_4(HPBA)_2(\mu\text{-}CH_3COO)_2(\mu\text{-}O)(\mu\text{-}OH)(OH_2)_2]ClO_4{\cdot}5H_2O$, a structural mimic of the active site of PAP [15]. Although it is believed that PAPs are only active in the heterovalent state [16], phosphatase activity has been reported for a number of diferric model complexes [17–23]. It was therefore of interest to study the hydrolase activity promoted by $[Fe_4(HPBA)_2(\mu\text{-}CH_3COO)_2(\mu\text{-}O)(\mu\text{-}OH)(OH_2)_2]ClO_4{\cdot}5H_2O$ and compare that activity with the activity of classic heterobinuclear $[Fe(III)(\mu\text{-}CH_3COO)_2(\mu\text{-phenoxide})M(II)]^+$ PAP biomimetics. In addition, we have investigated a new approach to the analysis of the typical bell-shaped pH–rate profiles reported for many biomimetic systems [8, 9, 17–25], particularly those for which more than two deprotonation equilibria are considered as part of the profile [9, 13, 14].

Materials and methods

All reagents and solvents were obtained commercially and were used without further purification.

Mass spectrometry

Low- and high-resolution positive-ion mass spectra were obtained using a Finnigan MAT 900 XL or a Voyager DE STR matrix-assisted laser desorption/ionization time-of-flight (MALDI-TOF) mass spectrometer in acetonitrile/water (1:1), pH 6.5.

Kinetic assays

Phosphatase-like activity using the activated phosphodiester substrate BDNPP [26] was measured between pH 5 and 10 in acetonitrile/buffer (1:1) with a multicomponent buffer system composed of 50 mM 2-(*N*-morpholino)ethanesulfonic acid (MES), 4-(2-hydroxyethyl)-1-piperazineethanesulfonic acid (HEPES) and 2-(*N*-cyclohexylamino) ethanesulfonic acid (CHES), with 250 mM $LiClO_4$. Complex concentrations of 20 μM were used, with 5 mM substrate used in pH-dependence and complex-dependence measurements, and a range of substrate concentrations between 1 and 9.2 mM were employed to measure the

Fig. 2 Ligands H_3HPBA and $H_2BPBPMP$ [8, 15]

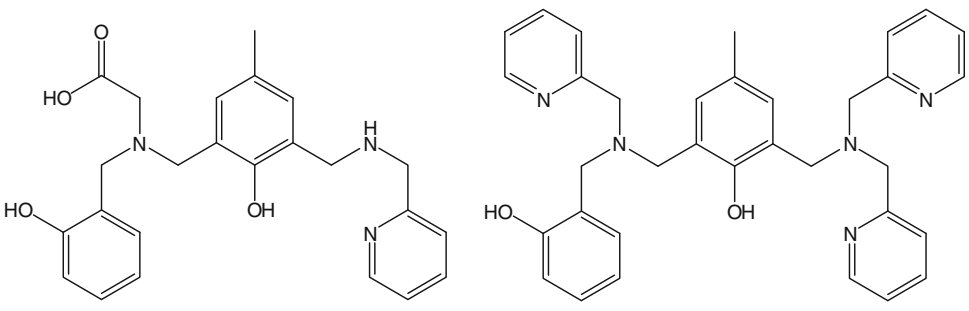

H_3HPBA **$H_2BPBPMP$**

substrate dependence of activity. Product formation was determined by measuring the change in absorption at 400 nm ($\varepsilon = 12{,}100\ M^{-1}\ cm^{-1}$) [13]. The initial-rate method was employed. Assays were performed such that the initial linear portion of the data was used for analysis. For each assay, corrections for the rate of autohydrolysis were applied. All data were fit using SigmaPlot [27].

Spectrophotometric titrations

Spectrophotometric experiments were performed at 24 °C with a U-1800 Hitachi spectrophotometer with 1-cm quartz cuvettes. The absorption spectra were obtained within the range 350–850 nm. A multicomponent buffer system was employed over a pH range from 4.6 to 10.0 with buffer concentrations of 50 mM for each of MES, CHES and HEPES and a constant ionic strength of 250 mM $LiClO_4$. The cuvette contained 0.05 mL complex (1.57 mM in acetonitrile), 0.5 mL buffer and 0.45 mL acetonitrile. All experiments were therefore carried out at a final complex concentration of 0.0789 mM in acetonitrile/water (1:1, v/v). The absorption spectrum for acetonitrile/water (1:1, v/v) was used as a baseline. Curve fitting of the data was completed using the program SPECFIT [28].

Syntheses of the ligand and metal complex

The ligand 2-((2-hydroxy-5-methyl-3-((pyridine-2-ylmethylamino)methyl)benzyl)(2-hydroxybenzyl)amino)acetic acid (H_2HPBA) and the complex $[Fe_4(HPBA)_2(\mu\text{-}CH_3COO)_2(\mu\text{-}OH)(\mu\text{-}O)(OH_2)_2]ClO_4{\cdot}8H_2O$ were prepared as described previously [15].

Caution: care should be taken when using the potentially explosive perchlorate anion.

Results

Solid-state structure

The structure of the complex $[Fe_4(HPBA)_2(\mu\text{-}CH_3COO)_2(\mu\text{-}OH)(\mu\text{-}O)(OH_2)_2]ClO_4{\cdot}8H_2O$ has been described previously [15]. In the solid state, each iron centre is six-coordinate, with a harder chromophoric NO_5 site comprising oxygen donors from the terminal and bridging phenolates, the carboxylate, the acetate ligand, a bridging hydr/oxo and the tertiary amine nitrogen donor. The softer N_2O_4 site has a water ligand, the bridging phenolate and acetate ligands, the secondary amine and the pyridine nitrogen as well as the bridging hydr/oxo. The dimers are bridged by a μ_4-$(OHO)^{3-}$ moiety [29–31]. On the basis of the crystallographic, susceptibility and Mössbauer studies, all metal ions are in the trivalent oxidation state [15].

Mass spectrometry

The MALDI-TOF mass spectrum was recorded under the solvent conditions (1:1 acetonitrile/water, pH 6.5) used in the kinetic studies. Under these conditions the dimeric species $[Fe(III)_2(HPBA)(\mu\text{-}CH_3COO)(H_2O)_2(OH)CH_3CN)]^+$ (m/z 683) and $[Fe(III)_2(HPBA)(H_2O)(OH)(CH_3CN)(ClO_4)]^+$ (m/z 705) were apparent, with no evidence for the tetrameric species.

Spectrophotometric titrations

An aqueous acetonitrile solution (1:1) of the complex was titrated in a multicomponent buffer over the pH range 4 4.6–10.0. Distribution curves obtained by fitting the absorbance versus pH data [28] suggested that there were four species (Fig. 3), associated through protonation/deprotonation equilibria, present in the solution over this pH range with three pK_a values of 4.9, 6.7 and 8.6.

Phosphatase-like kinetics

The phosphatase-like activity promoted by the $[Fe_4(HPBA)_4(\mu\text{-}CH_3COO)_2(\mu\text{-}OH)(\mu\text{-}O)(OH_2)_2]ClO_4$ complex in 1:1 acetonitrile/water was measured using the substrate BDNPP. The complex dependence of the hydrolytic activity was measured at pH 6.5 with a BDNPP concentration of 5 mM. The complex dependence was linear in the region 0–35 μM, with curvature of the plot observed at higher complex concentrations (35–50 μM) (Fig. 4). Subsequent analyses were undertaken at complex concentrations of 20 μM, within the linear part of the curve.

The substrate-concentration dependence of catalysis was also measured at pH 6.5 (Fig. 5). Michaelis–Menten-type behaviour was observed and the data were fitted using non-linear least-squares analysis to give a Michaelis constant (K_M) of 7.4 ± 0.6 mM and $V_{max} = 3.23 \times 10^{-8}\ M\ s^{-1}$, with k_{cat} (V_{max}/[complex]) = 1.6 ± 0.2 × $10^{-3}\ s^{-1}$.

The dependence of catalysis on pH was measured from pH 5 to 10, resulting in a bell-shaped pH–rate profile but with a limiting rate at high pH (Fig. 6). The data were fit separately to three equations (Eqs. 1, 2, 3):

$$V = V_0\left[\frac{1}{\left(1+\frac{[H^+]}{K_{a1}}+\frac{K_{a2}}{[H^+]}\right)}\right] \quad (1)$$

$$V = V_0\left[\frac{\left(1+\frac{\gamma K_{a2}}{[H^+]}\right)}{\left(1+\frac{[H^+]}{K_{a1}}+\frac{K_{a2}}{[H^+]}\right)}\right] \quad (2)$$

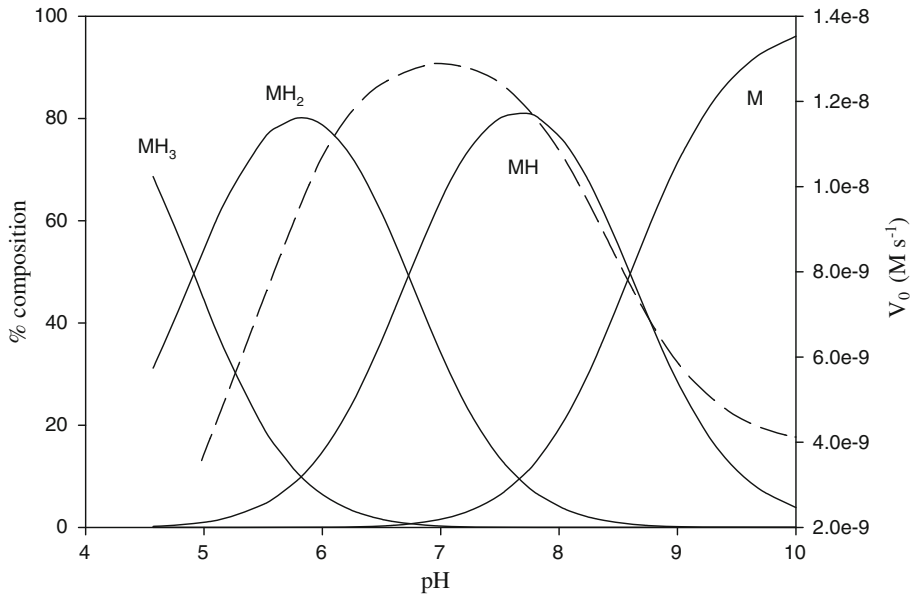

Fig. 3 Species distribution curve as a function of pH. The *solid lines* represent complex species (MH_3, MH_2, MH and M; vide infra Fig. 7), whereas the *broken line* is the pH profile of the complex (with initial rates shown on the *right-hand axis*). Studies were performed in aqueous acetonitrile (1:1) in a multicomponent buffer system

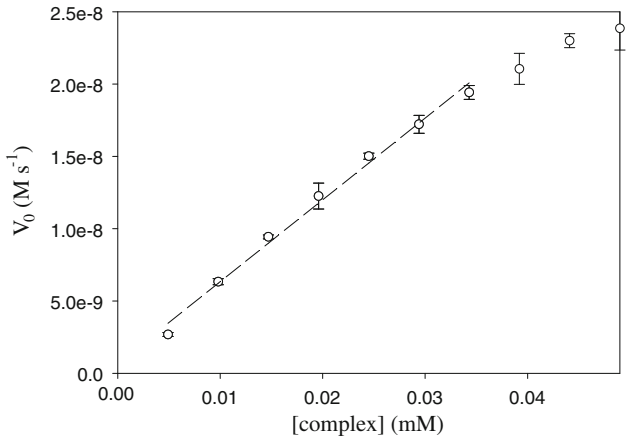

Fig. 4 Dependence of 2,4-bis(dinitrophenyl)phosphate (BDNPP) cleavage by the complex at pH 6.5, 25 °C, 5 mM BDNPP, acetonitrile/buffer (1:1) with 50 mM 2-(*N*-morpholino)ethanesulfonic acid (MES), 4-(2-hydroxyethyl)-1-piperazineethanesulfonic acid (HEPES) and 2-(*N*-cyclohexylamino)ethanesulfonic acid (CHES), and 250 mM $LiClO_4$) (*broken line* 0.005–035 mM)

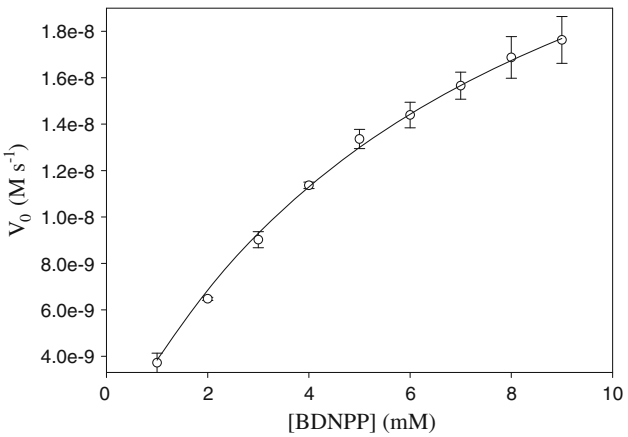

Fig. 5 Substrate dependence measured at pH 6.5 for 20 μM complex, acetonitrile/buffer (1:1) with 50 mM MES, HEPES and CHES, and 250 mM $LiClO_4$

$$V = V_0 \left[\frac{\left(1 + \frac{\alpha[H^+]}{K_{a2}} + \frac{\beta K_{a3}}{[H^+]}\right)}{\left(1 + \frac{[H^+]}{K_{a2}} + \frac{K_{a3}}{[H^+]} + \frac{[H^+]^2}{K_{a1}K_{a2}}\right)} \right]. \quad (3)$$

Equation 1 is the typical expression used to describe a symmetric bell-shaped profile [32–35]. Equation 2 was derived using a model based on the rapid-equilibrium diprotic model [34] and describes a reaction scheme (Fig. 7a) with two pK_a values and two catalytically active species in which the activity at high pH does not decrease to zero and where the activity of the species at higher pH is related to the activity of the species at optimum pH by the constant γ [34]. Equation 3 was again derived on the basis of the rapid equilibrium model [34], but now encompassing three pK_a values and three catalytically active species where the activity at high pH reaches a limit (Fig. 7b) [34]. The results of the fits of each equation are shown in Fig. 6. In each case the catalytically relevant pK_a values were determined (Table 1).

Discussion

The pH dependence of the catalytic activity with the substrate BDNPP displayed a bell-shaped profile with low but significant activity above pH ~ 9.5 (Fig. 6). Bell-shaped pH–rate profiles are, in the case of an enzyme with two ionizable groups, explained in the low-pH region (below the pH maximum) in terms of the increased hydrogen ion

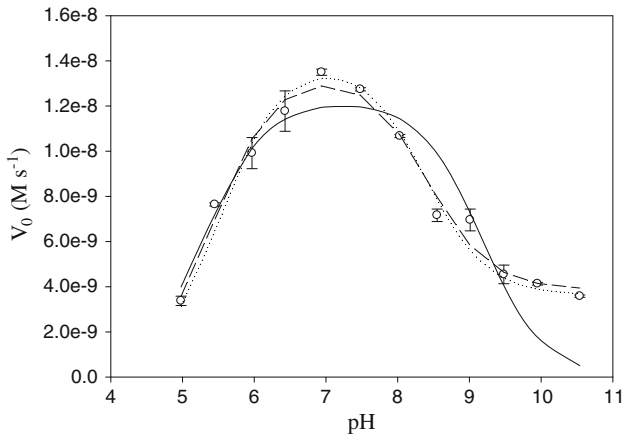

Fig. 6 pH dependence of the reaction rate for BDNPP hydrolysis by 20 μM complex in acetonitrile/buffer (1:1) with 50 mM MES, HEPES, and CHES, and 250 mM $LiClO_4$ (*circles* experimental points, *solid line* data fitted with Eq. 1, *broken line* data fitted with Eq. 2 and *dotted line* data fitted with Eq. 3)

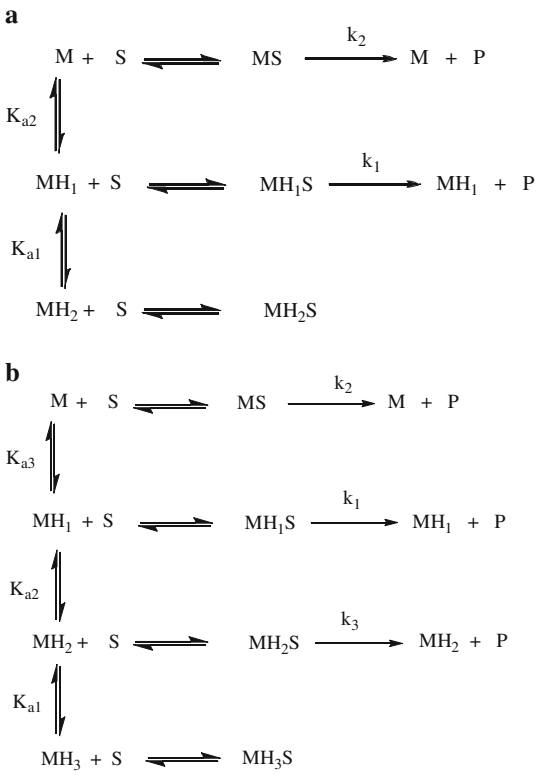

Fig. 7 Proposed **a** diprotic and **b** triprotic equilibrium schemes for species active at high and low pH [32–34, 36, 37]

concentration driving the enzyme into inactive protonated forms; in the high-pH region, above the pH maximum, the enzyme is driven towards inactive deprotonated forms [32–35]. In the case of dimeric Fe(III) biomimetic complexes the profile is usually ascribed to the sequential formation of species such as $Fe(H_2O)$–$Fe(H_2O)$/$Fe(H_2O)$–Fe(OH) and $Fe(H_2O)$–Fe(OH)/Fe(OH)–Fe(OH) invoking two deprotonation steps, and the kinetic data are fitted on the basis of determining the magnitudes of the two pK_a values under the assumption that the fully deprotonated form is inactive [8, 9, 17–25]. Other models invoking three deprotonation steps derived from potentiometric data have been reported, for example

$$\left[(OH_2)Fe(III)(OH_2)(L)M_B(OH_2)\right]/\left[(OH)Fe(III)(OH_2)(L)M_B(OH_2)\right] \quad pK_{a1}$$

$$\left[(OH)Fe(III)(OH_2)(L)M_B(OH_2)\right]/\left[(OH)Fe(III)(\mu\text{-}OH)(L)M_B(OH_2)\right] \quad pK_{a2}$$

$$\left[(OH)Fe(III)(\mu\text{-}OH)(L)M_B(OH_2)\right]/\left[(OH)Fe(III)(\mu\text{-}OH)(L)M_B(OH)\right] \quad pK_{a3}.$$

Here, L is $BPBPMP^{2-}$ and M_B is Zn (pK_{a1} 4.86, pK_{a2} 6.00, pK_{a3} 7.22), Ni (pK_{a1} 5.3, pK_{a2} 6.80, pK_{a3} 8.61), Cu (pK_{a1} 5.25, pK_{a2} 6.20, pK_{a3} 7.82) or Co (pK_{a1} 5.00, pK_{a2} 6.58, pK_{a3} 8.31) [9, 11, 13, 14]. In these cases the bell-shaped pH–rate profiles were fitted such that only pK_{a1} and pK_{a3} (the low-pH and high-pH extrema) were included in the analysis but not pK_{a2}, representing an intermediate species. Furthermore, the commonly observed situation of a limiting rate at high pH was not usually considered. The presence of an active species obscured within a bell-shaped pH–rate profile is not without precedence in metalloenzyme systems. Studies of the pH–rate profiles of *Klebsiella aerogenes* and *Canavalia ensiformis* urease suggested that a third catalytically relevant species was present, with a pK_a falling between the high-pH and low-pH pK_a values observed directly in the bell-shaped profiles [36, 37].

Fitting the data in the present case to an equation (Eq. 1) usually employed for bell-shaped pH–rate profiles gave a poor fit (Fig. 6). Considerably better fits were obtained with equations which took account of the limiting rate observed at high pH (Eqs. 2, 3). In each case the pK_{a1} calculated was constant (Table 1). The high-pH pK_a (pK_{a3}) was consistent using Eqs. 2 and 3 (8.41 and 8.38, respectively) but was overestimated with Eq. 1 (9.17); in addition, the limiting rate at high pH was poorly modelled. The fit with Eq. 3, which accounts for three reaction pathways, interrelated by three deprotonation steps, contributing to the hydrolysis reaction (Fig. 7b) resulted in pK_a values (5.3, 6.2 and 8.4) in reasonable accord with the values determined from the spectrophotometric analysis (Fig. 3). The result suggests that in the pH range 5–10 two species contribute to the hydrolysis, with a third being responsible for the residual activity seen above pH ~ 9.5. In the present case the use of the classic bell-shaped expression (Eq. 1) is clearly insufficient to fit the data. In terms of the simplest expression, clearly Eq. 2 gives an appropriate fit to the data. However, employing an expression such as Eq. 3 produces information about the "obscured" entity.

Table 1 pK_a values and coefficients derived from the fit of the pH–rate profile data and spectrophotometric titration

	pK_{a1}	pK_{a2}	pK_{a3}	Coefficients (Eqs. 2, 3)	Rate constants (Fig. 7) ($M\ s^{-1}$)
Equation 1	5.29		9.17		
Equation 2	5.42		8.41	$V_0 = k_1$	$k_1 = 1.40 \times 10^{-8}$
				$\gamma = 0.28$	$k_2 = 0.40 \times 10^{-8}$
Equation 3	5.37	6.06	8.38	$V_0 = k_1$	$k_1 = 1.40 \times 10^{-8}$
				$\alpha = k_3/k_1 = 0.79$	$k_2 = 0.40 \times 10^{-8}$
				$\beta = k_2/k_1 = 0.28$	$k_3 = 1.11 \times 10^{-8}$
Spectrophotometric	4.9	6.7	8.6		

pK_{a1} is the low-pH pK_a, pK_{a3} is the high-pH pK_a and pK_{a2} is ascribed to the "hidden" species

There is considerable literature precedence for the assignment of the pK_a values [13, 14, 17–21, 23]. As described above, the pK_a of approximately 5 is assigned to $Fe(H_2O)$–$Fe(H_2O)$/$Fe(H_2O)$–Fe(OH), with pK_{a2} of approximately 6.5 assigned to the deprotonation of Fe(III)–H_2O with subsequent formation of an Fe–(μ-OH)-Fe moiety [17]. pK_{a3} of approximately 8.4 is assigned to the deprotonation of a water molecule bound to the second Fe(III) [20]. The presence of the three deprotonation steps suggests that the precursor species is of the form $[(H_2O)Fe(H_2O)Fe(H_2O)]_x^{n+}$ ($x = 1$ or 2), with the fully deprotonated form responsible for the low but significant activity above pH $\sim$ 9.5 (Fig. 6) [14]. The model predicts that at high pH the active species retains sufficient coordination flexibility to permit coordination of BDNPP, but the low rate is likely to be due to the slow exchange rate of hydroxide at the substrate binding site. Nonetheless, the rate at high pH is still several orders of magnitude greater than both the spontaneous rate, and the rate for the free Fe(III). Clearly, the nucleophilic agent promoting the hydrolysis of the BDNPP substrate is an Fe(III)–OH species.

Catalytically active tetrameric Fe(III) and Ni(II) complexes have been reported [38, 39]. The iron complex has been shown to be a promoter of ATP hydrolysis [38] and the nickel complex has been investigated for its potential to hydrolyze bis(nitrophenyl)phosphate [39]. Although ^1H NMR spectroscopy was employed to confirm the structure of the former complex in solution, no evidence for the composition of the catalytically active Ni(II) complex was reported. In the present case, a number of options for the catalytically active entity in solution can be considered, including the intact tetramer and a dimer resulting from cleavage of the μ-OH/μ-O bridges. In both cases loss of the bridging acetates would be anticipated under the conditions of catalysis [9, 10, 12–14, 23, 25] to form $[Fe_4(HPBA)_2(\mu\text{-OH})(\mu\text{-O})(OH_2)_6]^+$ and/or $[(OH_2)_2Fe(HPBA)Fe(OH_2)_3]^{3+}$ (Fig. 8); subsequent deprotonations would lead to $[(OH_2)Fe(HPBA)(\mu\text{-OH})Fe(H_2O)_2]^{+/2+}$, with the $Fe(H_2O)$–$Fe(H_2O)$/$Fe(H_2O)$–Fe(OH) and $Fe(H_2O)$–Fe(OH)/Fe(OH)–Fe(OH) combinations necessary for catalytic activity [17–19, 21]. Some support for the assignment of the catalytically active entity being a dimer arises from the investigation of the dependence of the complex concentration on

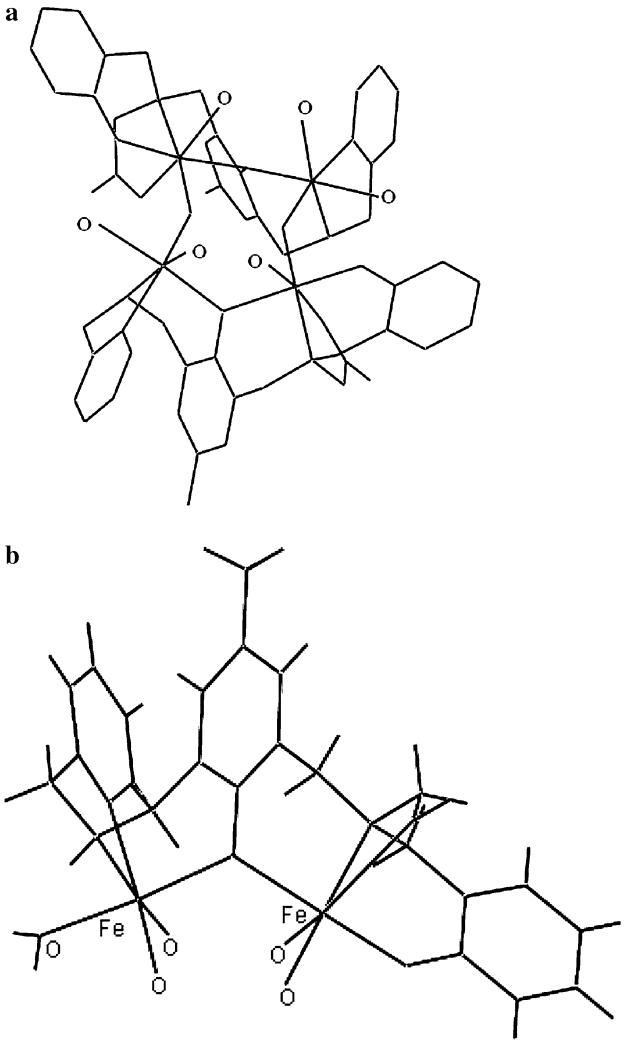

Fig. 8 **a** Proposed structure of $[Fe_4(HPBA)_2(\mu\text{-O})(\mu\text{-OH})(OH_2)_2]^{3+}$ and **b** proposed structure of $[Fe_2(HPBA)(OH_2)_5]^{3+}$ (*O* signifies a water molecule) [15]

Table 2 Kinetic parameters of heterovalent and homovalent complexes

Complex	k_{cat} (s^{-1})	K_M (mM)	pH optimum
[Fe(III)Cu(II)(BPBPMP)(μ-$CH_3COO)_2$](ClO_4) [9]	1.77×10^{-3}	11	7
[Fe(III)Mn(II)(BPBPMP)(μ-$CH_3COO)_2$](ClO_4) [12]	4.51×10^{-4}	2.1	6.7
[Fe(III)Ni(II)(BPBPMP)(μ-$CH_3COO)_2$](ClO_4) [13]	4.47×10^{-4}	3.85	6
[Fe(III)Zn(II)(BPBPMP)(μ-$CH_3COO)_2$](ClO_4) [14]	7.31×10^{-4}	8.1	6.1
[Ga(III)Zn(II)(BPBPMP)(μ-$CH_3COO)_2$](ClO_4) [25]	1.41×10^{-3}	7.15	6.8
[Fe(III)(OH_2)(μ-OH)Zn(II)(BPBPMP)]($ClO_4)_2$ [24]	9.13×10^{-4}	4.2	6.5

H_2BPBPMP is 2-((bis(pyridin-2-ylmethyl)amino)methyl)-6-(((2-hydroxybenzyl)(pyridin-2-ylmethyl)amino)methyl)-4-methylphenol (Fig. 2)

the hydrolysis reaction. The complex-concentration dependence was linear at low concentrations, with deviation from linearity at higher complex concentrations (Fig. 4). Similar non-linear complex-concentration dependence has been observed previously for the reaction of an Fe(III)Fe(III) complex with BDNPP [19]. In that case the data were analysed, employing linearization by the Lineweaver–Burk method of an expression which assumed an initial equilibrium step to form a substrate–catalyst complex, with a subsequent kinetic step [19]. Analysis by the same method in the present case did not result in a linear relationship over the range of the complex concentration, suggesting more complicated, e.g. dimer–tetramer equilibria, behaviour, being responsible for the observed curvature. The mass-spectral evidence, the complex-concentration dependence and the similarity of the kinetic parameters ($K_M = 7.4 \pm 0.6$ mM; $k_{cat} = 1.6 \pm 0.2 \times 10^{-3}$ s^{-1}) with those reported for a series of dimeric complexes (Table 2) suggest that a dimeric form of the complex is the active entity under the catalytic conditions [9, 12–14, 24, 25], mimicking the previously reported forms of catalytically active species in the heterovalent PAP model [Fe(III)Fe(II)(BPBPMP)(OH)(O)]$^+$.

Conclusions

The question does arise, however, as to how relevant these Fe(III) complexes are as models for the mammalian PAPs. For the Fe(III)Fe(III) form of uteroferrin an upper limit of less than 1% of the activity of the heterovalent form has been determined [16], the release of the ultimate reaction product (phosphate) being proposed as the likely candidate for the rate-limiting step in the PAP-catalyzed reaction [1, 18, 25, 40]. This hypothesis finds support in the relative water exchange rates of Fe(III) and Fe(II) (10^2 and 10^6 s^{-1}, respectively) [41–43]. The diferric model reported here is active and is, in some ways, a model for the oxidized PAP. Mechanistically however, the oxidized system is indistinguishable from the reduced model systems, indicating that the oxidation state of the diiron centre is only important in the enzymic systems that are substantially faster. Since hydrolysis is so slow in the models, the exchange of substrate is not significant in catalysis.

More significant though is the analysis of the phosphatase activity of the complex. The more rigorous analysis of the bell-shaped pH–rate profile proposed herein suggests that in similar systems reported previously the analysis of the observed bell-shaped pH–rate profiles was not sufficiently thorough, particularly in those systems in which the rate at high pH approaches a finite value.

Acknowledgments This work was funded by a grant from the Australian Research Council (DP0986292).

References

1. Mitić N, Smith SJ, Neves A, Guddat LW, Gahan LR, Schenk G (2006) Chem Rev 106:3338–3363
2. Klabunde T, Krebs B (1997) Struct Bonding (Berlin) 89:177–198
3. Antanaitis BC, Aisen P, Lilienthal HR (1983) J Biol Chem 258:3166–3172
4. Averill BA, Davis JC, Burman S, Zirino T, Sandersloehr J, Loehr TM, Sage JT, Debrunner PG (1987) J Am Chem Soc 109:3760–3767
5. Yang YS, McCormick JM, Solomon EI (1997) J Am Chem Soc 119:11832–11842
6. Wang DL, Holz RC, David SS, Que L, Stankovich MT (1991) Biochemistry 30:8187–8194
7. Bernhardt PV, Schenk G, Wilson GJ (2004) Biochemistry 43:10387–10392
8. Neves A, de Brito MA, Drago V, Griesar K, Haase W (1995) Inorg Chim Acta 237:131–135
9. Lanznaster M, Neves A, Bortoluzzi AJ, Aires VVE, Szpoganicz B, Terenzi H, Severino PC, Fuller JM, Drew SC, Gahan LR, Hanson GR, Riley MJ, Schenk G (2005) J Biol Inorg Chem 10:319–332
10. Schenk G, Peralta RA, Batista SC, Bortoluzzi AJ, Szpoganics B, Dick AK, Herrald P, Hanson GR, Szilagyi RK, Riley MJ, Gahan LR, Neves A (2008) J Biol Inorg Chem 13:139–155
11. Xavier RF, Neves A, Casellato A, Peralta RA, Bortoluzzi AJ, Szpoganicz B, Severino PC, Terenzi H, Tomkowicz Z, Ostrovsky S, Haase W, Ozarowski A, Krzystek J, Telser J, Schenk G, Gahan LR (2009) Inorg Chem 48:7905–7921
12. Karsten P, Neves A, Bortoluzzi AJ, Lanznaster M, Drago V (2002) Inorg Chem 41:4624–4626
13. Batista SC, Neves A, Bortoluzzi AJ, Vencato I, Peralta RA, Szpoganicz B, Aires VVE, Terenzi H, Severino PC (2003) Inorg Chem Commun 6:1161–1165

14. Lanznaster M, Neves A, Bortoluzzi AJ, Szpoganicz B, Schwingel E (2002) Inorg Chem 41:5641–5643
15. Boudalis AK, Aston RE, Smith SJ, Mirams RE, Riley MJ, Schenk G, Blackman AG, Hanton LR, Gahan LR (2007) Dalton Trans 5132–5139
16. Merkx M, Averill BA (1998) Biochemistry 37:11223–11231
17. Horn A, Vencato I, Bortoluzzi AJ, Horner R, Silva RAN, Szpoganicz B, Drago V, Terenzi H, de Oliveira MCB, Werner R, Haase W, Neves A (2005) Inorg Chim Acta 358:339–351
18. Duboc-Toia C, Menage S, Vincent J-M, Averbuch-Pouchot MT, Fontecave M (1997) Inorg Chem 36:6148–6149
19. Longhinotti E, Domingos JB, Szpoganicz B, Neves A, Nome F (2005) Inorg Chim Acta 358:2089–2092
20. Parrilha GL, Fernandes C, Bortoluzzi AJ, Szpoganicz B, Silva MdS, Pich CT, Terenzi H, Horn A (2008) Inorg Chem Commun 11:643–647
21. Verge F, Lebrun C, Fontecave M, Menage S (2003) Inorg Chem 42:499–507
22. Liu C, Yu S, Li D, Liao Z, Sun X, Xu H (2002) Inorg Chem 41:913–922
23. Neves A, Terenzi H, Horner R, Horn A, Szpoganicz B, Sugai J (2001) Inorg Chem Commun 4:388–391
24. Neves A, Lanznaster M, Bortoluzzi AJ, Peralta RA, Casellato A, Castellano EE, Herrald P, Riley MJ, Schenk G (2007) J Am Chem Soc 129:7486–7487
25. Smith SJ, Casellato A, Hadler KS, Mitić N, Riley MJ, Bortoluzzi AJ, Szpoganicsz B, Schenk G, Neves A, Gahan LR (2007) J Biol Inorg Chem 12:1207–1220
26. Bunton CA, Farber SJ (1969) J Org Chem 34:767–772
27. Systat Software (2006) SigmaPlot for Windows, version 10. Systat Software, San Jose
28. Binstead RA, Zuberbuhler AD (1993–1995) SPECFIT: a program for global least squares fitting of equilibria and kinetics systems using factor analysis and Marquardt minimization, version 2.09. Spectrum Software Associates, Chapel Hill
29. Boudalis AK, Lalioti N, Spyroulias GA, Raptopoulou CP, Terzis A, Bousseksou A, Tangoulis V, Tuchagues J-P, Perlepes SP (2002) Inorg Chem 41:6474–6487
30. Stibrany RT, Gorun SM (1990) Angew Chem 102:1195–1197
31. Gorun SM, Stibrany RT, Lillo A (1998) Inorg Chem 37:836–837
32. Purich DL, Allison RD (2000) Handbook of biochemical kinetics. Academic Press, San Diego, p 544
33. von Euler H, Josephson K, Myrback K (1924) Z Physiol Chem 134:39–49
34. Segel IH (1975) Enzyme kinetics: behavior and analysis of rapid equilibrium and steady-state enzyme systems. Wiley-Interscience, New York
35. Mitić N, Valizadeh M, Leung EWW, de Jersey J, Hamilton S, Hume DA, Cassady AI, Schenk G (2005) Arch Biochem Biophys 439:154–164
36. Mulrooney S, Zakharian T, Schaller RA, Hausinger RP (2001) Arch Biochem Biophys 394:280–282
37. Krajewska B, Ciurli S (2005) Plant Physiol Biochem 43:651–658
38. Li D-F, Liao Z-R, Wei Y-G, Wang M, Chen W-X, Li W-K, Mao X-A (2003) Dalton Trans 2164–2169
39. Sung N, Kim T-Y (2006) Agric Chem Biotechnol 49:86–89
40. Twitchett MB, Schenk G, Aquino MAS, Yiu DTY, Lau TC, Sykes AG (2002) Inorg Chem 41:5787–5794
41. Helm L, Merbach AE (2005) Chem Rev 105:1923–1959
42. Tanaka L, Yamada S (1976) J Chem Soc Chem Commun 178–179
43. Grant M, Jordan R (1981) Inorg Chem 20:55–60